ELSEVIER

International Journal of Solids and Structures 41 (2004) 5885–5901

INTERNATIONAL JOURNAL OF SOLIDS and STRUCTURES

www.elsevier.com/locate/ijsolstr

Micromechanics of shear bands

B.S. Gardiner [a,*], A. Tordesillas [b,*]

[a] Department of Civil and Environmental Engineering, University of Melbourne, Parkville VIC 3010, Australia
[b] Department of Mathematics and Statistics, University of Melbourne, Parkville, Melbourne, VIC 3010, Australia

Received 31 October 2003; received in revised form 21 April 2004
Available online 17 July 2004

Abstract

In the past, we have developed a *micromechanically-based* constitutive model of a 2D, monodisperse granular assembly consisting of circular particles, in which the tangential displacements at particle–particle contacts were limited to microslip only i.e. particles do not slide relative to each other. This constitutive law was later extended, using slightly more advanced contact laws, to include sliding contacts, along with the potential for loss of contacts. Furthermore, through these contact laws, evolution of the distribution of contact modes (non-sliding or microslip contacts, sliding contacts and loss of contacts), contact forces and the density of contact directions, can be determined as the deformation proceeds i.e. *deformation-dependent anisotropies*. In this paper we apply this latter constitutive model to shear band formation in a bi-axial test. Using an initially isotropic sample, we demonstrate that the constitutive model can reproduce the various anisotropies that have been observed in experiments and simulations. Moreover, the predicted shear band properties (e.g. thickness, inclination, prolonged localisation, void ratio) show even better agreement with experimental observations than previously found using our past models. These results take on particular significance when one considers that, in contrast to the constitutive equations traditionally used for granular materials, the micromechanically-based constitutive model presented here contains a direct link to the physical and measurable properties of particles (e.g. particle–particle friction coefficient, particle stiffness coefficients) and so arguably contains no fitting parameters.

Keywords: Micropolar; Micromechanics; Constitutive laws; Granular media; Anisotropy

1. Introduction

One of the difficulties encountered when handling granular matter is the lack of a well-accepted constitutive model. By now it should be widely acknowledged that the behaviour of granular materials is governed by the interaction between constituent particles. That is, the finite size of particles cannot be ignored in a continuum model. For example, the ability of particles to rotate significantly reduces the

* Corresponding authors. Tel.: +61-3-8344-9685; fax: +61-3-8344-4599 (B.S. Gardiner).
E-mail addresses: bgardine@unimelb.edu.au (B.S. Gardiner), a.tordesillas@ms.unimelb.edu.au (A. Tordesillas).

0020-7683/$ - see front matter © 2004 Elsevier Ltd. All rights reserved.
doi:10.1016/j.ijsolstr.2004.05.051

strength of granular materials (Oda et al., 1982). With this in mind, if we are to remain in a continuum setting, the classical models of plasticity need to be extended for granular materials to include, at the very least, the effects of a length-scale and particle rotation. This extension can be made within the framework of micropolar and/or higher order strain gradient theories. A less phenomenological approach would be to develop constitutive models based on averaging the discrete interactions between particles over a region, to obtain continuum laws. This is the approach taken here.

In this paper, a micromechanically based micropolar constitutive law is developed for two-dimensional, dry assemblies of uniformly-sized, circular particles. The homogenisation procedure used to obtain the constitutive law is the small strain scheme of Tordesillas and Walsh (2002) and is outlined here in Section 2. In particular, this scheme is considered high resolution, as it is based around the contacts of a single particle and its nearest neighbours to enable fine-scale structures to be captured. Section 3 introduces specific strain dependent contact laws into the homogenisation procedure, which incorporate sliding and non-sliding contacts, a rolling resistance and loss of contacts. These strain dependent contact laws are obtained from a mean-field approximation to the motion around a contact. Hence, these strain dependent contact laws naturally result in an *evolving* contact anisotropy and contact force anisotropy. To demonstrate this anisotropy development, the constitutive laws are presented in a form that assumes that the particle contacts are initially isotropically distributed in both direction and force. Finally, in Section 4, the problem of shear band formation and evolution in bi-axial test is studied to test the constitutive model. The shear band analysis adopted here is based on the method presented in Tordesillas et al. (in press). The method is a combination of the one-dimensional analysis first introduced for micropolar continua by Mühlhaus and Vardoulakis (1987), and an incremental step-by-step procedure for the post localisation analysis. Additionally, from the onset of deformation, the quantities defining the characteristics of the material (e.g. contact modes, contact anisotropy and contact force anisotropy) are updated in a stepwise manner after each small increment of strain. Although this method of shear band analysis is restrictive, in comparison for example to a finite element method, the semi-analytic solutions provided by the one-dimensional simplification help to identify the limitations of the shear band analysis versus the constitutive model (Tordesillas et al., 2003).

2. The micropolar homogenisation scheme

Recently, Tordesillas and Walsh (2002) derived two-dimensional expressions to link discrete quantities, such as the relative particle motion, contact forces $\mathbf{f}$ and contact moments M, to the micropolar continuum concepts of stress $\boldsymbol{\sigma}$, couple stress $\boldsymbol{\mu}$, strain $\boldsymbol{\varepsilon}$ and curvature (gradient in rotations) $\boldsymbol{\kappa}$. Their approach differs from many previous homogenisation methods in that it is based on averaging the discrete quantities over only a small particle cluster consisting of just a single particle and its immediate neighbours (the first ring). The expressions obtained by Tordesillas and Walsh (2002) were:

$$\sigma_{\alpha\beta} = \frac{1}{\pi R(1+v)} \int_{\Omega} f_{\alpha} n_{\beta} \Phi \, \mathrm{d}n, \tag{2.1}$$

$$\mu_{\alpha} = \frac{1}{\pi R(1+v)} \int_{\Omega} [M n_{\alpha} + \mathrm{Re}_{\beta\phi 3} f_{\beta} n_{\alpha} n_{\phi}] \Phi \, \mathrm{d}n. \tag{2.2}$$

In the above expressions, R represents the radius of circular particles (i.e. a monodisperse system), v represents the void ratio of the Voronoi cell associated with the particle cluster (ratio of the area of the void to the area of the particle), n_{α} is the α-component of the unit vector $\mathbf{n}$ describing the direction of the contact from the particle centre, $e_{\beta\phi 3}$ is the permutation symbol and Ω represents all possible orientations in two-dimensional space. A repeated subscript signifies a summation over the range of the repeated subscript.

Finally, the contact density distribution function Φ describes the expectation of finding a contact in a given direction. For a particle with N contacts,

$$\int_{\Omega} \Phi \, \mathrm{d}n = N. \tag{2.3}$$

Note, both the contact moments and the contact forces contribute to the couple stress in (2.2).

Eqs. (2.1) and (2.2) can be used to construct micromechanically-based, micropolar constitutive models for monodisperse granular materials once (i) a link is established between the discrete quantities and deformation e.g. between contact force and strain, and (ii) the probable distribution of contact orientations, i.e. Φ, is completely known. Obviously, both of these requirements pose significant challenges. However, the first of these requirements can be tackled by introducing a simple, well-known, set of contact laws which link contact forces and moments to the relative displacement and rotation of contact points. Homogenisation or averaging techniques must then be employed to relate the relative motion at contacts to the continuum properties of strain and curvature. This procedure will be discussed later in Section 3. The following discussion will concentrate on the second requirement, namely that of linking *contact anisotropy* with deformation, which arguably poses a far greater challenge.

The form of the contact anisotropy remains an open problem and is an area that is currently attracting considerable research (e.g. Rothenburg et al., 1989; Chapter 4 of Oda and Iwashita, 1999; Nouguier-Lehon et al., 2003; Kruyt and Rothenburg, 2003; Luding, 2003). An expression commonly fitted to experimental and simulation data for the contact anisotropy is

$$\Phi(\mathbf{n}, \mathbf{m}, \chi, v) = \frac{N}{2\pi}(1 + \chi \cos(2\theta)), \tag{2.4}$$

where χ is the degree of contact anisotropy and can take values in the range $0 < \chi \leqslant 1$. The symbol θ is defined by $\cos\theta = \mathbf{m} \cdot \mathbf{n}$, where the 'dot' denotes the scalar product, and $\mathbf{m}$ is the unit vector pointing in the direction of greatest probability of finding a contacting neighbour. The evolution of the contact anisotropy can then be incorporated into (2.1) and (2.2) by linking N and χ to the deformation. The obvious drawback of this approach is that, unless a universal contact anisotropy evolution law is available, the resulting constitutive equation will be unique to each application, as the evolution of the fabric has been restricted to a predefined mode of deformation. This may compromise a model's generality and its ability to predict novel anisotropies arising in highly localised structures like shear bands. One of the main aims of the current paper is to show that contact anisotropy need not be predefined. In fact, we propose that the contact laws alone can provide enough anisotropy and evolution if they credibly account for the various modes of contact (non-sliding, sliding and loss of contacts). Moreover, the predicted evolution of the force and contact anisotropies are consistent with those observed in shear bands. To demonstrate or test this proposal, for the remainder of this paper we will set $\chi = 0$, which corresponds to an initially isotropic contact distribution.

3. Contact laws and the micromechanical constitutive model

Presented in this section are expressions used in Eqs. (2.1) and (2.2) to link contact forces and moments to particle motion, along with the resulting micromechanical constitutive model. The modification of these contacts laws from our earlier models will be discussed, to highlight the source of the current model's significantly improved predictive capabilities.

The normal force at a contact is assumed to consist of two parts: (i) the initial normal force at a contact, and (ii) the normal force resulting from a relative normal displacement of contacting particles. If contacts are assumed to be cohesionless and linear elastic, then

$$f^{\mathrm{n}} = \begin{cases} f^{\mathrm{initial}} + k^{\mathrm{n}}\Delta u^{\mathrm{n}} & \text{if } f^{\mathrm{initial}} + k^{\mathrm{n}}\Delta u^{\mathrm{n}} < 0 \quad \Rightarrow \text{evolving normal contact force} \\ 0 & \text{if } f^{\mathrm{initial}} + k^{\mathrm{n}}\Delta u^{\mathrm{n}} \geqslant 0 \quad \Rightarrow \text{no contact} \end{cases} \tag{3.1}$$

where f^{initial} is the initial normal contact force, k^{n} is the particle's normal stiffness coefficient, and Δu^{n} is the relative normal displacement of contact points between two contacting particles. The previous models of Tordesillas and Walsh (2002); Walsh and Tordesillas (2002); Tordesillas et al. (in press) assumed a constant f^{n}, that is $k^{\mathrm{n}} = 0$, and hence did not account for the evolution of the normal contact force or the potential for loss of contacts ($f^{\mathrm{initial}} + k^{\mathrm{n}}\Delta u^{\mathrm{n}} \geqslant 0$).

The initial normal contact force reflects the initial confinement imposed on the granular material at the boundaries (wall, experimental apparatus, free surface etc.). The initial normal contact force can contain any form of anisotropy, but in keeping with the aim expressed in the previous section of demonstrating how anisotropy can naturally arise from the current constitutive model, it is assumed that the normal contact force distribution is initially isotropic, namely

$$f^{\mathrm{initial}} = -\frac{\eta k^{\mathrm{n}} R}{2\pi}. \tag{3.2}$$

In other words, it is assumed that a particle initially experiences an equal compression in all directions of magnitude ηR. In general, η would be expected to be less than 10%, and for hard discs it would be more likely to be under 1%.

The above contact law incorporates the potential for loss of contacts as the deformation of the granular material proceeds. A loss of contact in certain directions will remove any contribution to the evaluation of (2.1) and (2.2) from the corresponding range of angles in Ω. This would have the same effect as choosing a contact density distribution function that is zero or "switched off" for angles in which particle contacts are broken. In other words, without modifying Φ, the effects of an evolving contact anisotropy have been incorporated through the contact law (3.1).

The tangential contact force can be approximated by following Coulomb's contact law, that is

$$f^{\mathrm{t}} = \begin{cases} \mathrm{sign}(\Delta u^{\mathrm{t}})\mu|f^{\mathrm{n}}| & \text{if } |k^{\mathrm{t}}\Delta u^{\mathrm{t}}| \geqslant |\mu f^{\mathrm{n}}| \text{ and } f^{\mathrm{n}} < 0 \quad \Rightarrow \text{sliding contact} \\ k^{\mathrm{t}}\Delta u^{\mathrm{t}} & \text{if } |k^{\mathrm{t}}\Delta u^{\mathrm{t}}| < |\mu f^{\mathrm{n}}| \text{ and } f^{\mathrm{n}} < 0 \quad \Rightarrow \text{non-sliding contact}, \\ 0 & \text{if } f^{\mathrm{n}} \geqslant 0 \quad \Rightarrow \text{no contact} \end{cases} \tag{3.3}$$

where μ is the inter-particle friction coefficient, k^{t} is the particle's tangential stiffness coefficient, and Δu^{t} is the tangential component of the relative displacement of the contact points. Note that the initial tangential contact force is assumed to be zero. This assumption may not be appropriate if, for example, the effect of gravity on the initial particle interaction is to be included. The previous models of Tordesillas and Walsh (2002) and Walsh and Tordesillas (2002) and Tordesillas et al. (in press) only considered non-sliding contacts.

A linear contact law is also used to approximate the rolling resistance for both sliding and non-sliding contacts,

$$M^{\mathrm{slid}} = k^{\mathrm{slid}}\Delta\omega, \text{ sliding contacts} \tag{3.4}$$

$$M^{\mathrm{no\,slid}} = k^{\mathrm{no\,slid}}\Delta\omega, \text{ non-sliding contacts} \tag{3.5}$$

where $\Delta\omega$ is the relative rotation at a contact, and k^{slid} and $k^{\mathrm{no\,slid}}$ are the coefficients of rolling stiffness for sliding and non-sliding contacts, respectively.

The above contact laws, Eqs. (3.1)–(3.5), are to be used in (2.1) and (2.2) to link the continuum quantities of stress and couple stress to the deformation, however, we still need to relate the discrete relative motion at contacts to the continuum quantities of strain and curvature. This link has been the topic of considerable research (e.g. Bagi, 1996; Chapter 1 of Oda and Iwashita, 1999; Dedecker et al., 2000; Bardet and Vardoulakis, 2001), with most studies concentrating on finding schemes to gain a sensible strain measure from the non-affine motions of a large number of particles. As our approach is based on quantities

averaged over a very small cluster of particles (consisting only of a single particle and its immediate neighbours), we expect that the corresponding strain measure is simpler. In fact, Tordesillas and Walsh (2002) already utilised a link between strain, curvature, relative displacement at a contact and the relative rotation at a contact, which was provided by Chang and Ma (1991). This method approximates the relative motion of two particles by a Taylor's series expansion about the contact point. For two circular particles, labelled 'a' and 'b', of radius R, the relative displacement Δu_α^{ab} and rotation $\Delta\omega^{ab}$ can be expressed as

$$u_\alpha^a = u_\alpha^b + 2Ru_{\alpha,\beta}^b n_\beta + \frac{(2R)^2}{2!}u_{\alpha,\beta\phi}^b n_\beta n_\phi + \cdots + \tag{3.6}$$

$$\omega^a = \omega^b + 2R\omega_{,\beta}^b n_\beta + \frac{(2R)^2}{2!}\omega_{,\beta\phi}^b n_\beta n_\phi + \cdots +, \tag{3.7}$$

where a comma within a subscript represents a partial derivative with respect to all the subscripts following the comma. Combining the following well-known expressions for the relative motion of two particles:

$$\Delta u_\alpha^{ab} = u_\alpha^a - u_\alpha^b + \mathrm{Re}_{\alpha\beta 3} n_\beta(\omega^a + \omega^b) \tag{3.8}$$

$$\Delta\omega^{ab} = \omega^a - \omega^b, \tag{3.9}$$

with (3.6) and (3.7), and keeping only the first order terms, leads to

$$\Delta u_\alpha = 2Ru_{\alpha,\beta}n_\beta + 2\mathrm{Re}_{\alpha\beta 3}n_\beta(\omega + R\omega_{,\phi}n_\phi) \tag{3.10}$$

$$\Delta\omega = 2R\omega_{,\alpha}n_\alpha. \tag{3.11}$$

In (3.10) and (3.11) the superscripts denoting particle labels have been dropped for generality. The micropolar strain and curvature are defined as,

$$\varepsilon_{\alpha\beta} = u_{\alpha,\beta} + e_{\alpha\beta 3}\omega \tag{3.12}$$

$$\kappa_\alpha = \omega_{,\alpha}, \tag{3.13}$$

respectively. Hence, from (3.10)–(3.13), the following links are obtained between the discrete and continuum deformation quantities:

$$\Delta u^{\mathrm{n}} = 2R\varepsilon_{\alpha\beta}n_\alpha n_\beta, \tag{3.14}$$

$$\Delta u^{\mathrm{t}} = 2R(\varepsilon_{\alpha\beta}n_\beta t_\alpha - Rn_\varphi\kappa_\varphi), \tag{3.15}$$

and

$$\Delta\omega = 2R\kappa_\alpha n_\alpha. \tag{3.16}$$

In (3.15), t_α is the α-component of the unit vector perpendicular to $\mathbf{n}$.

Eqs. (3.14)–(3.16) provide the link between the contact laws and the deformation. Hence (3.14) and (3.15) and the contact laws now give a deformation dependent contact force and moment anisotropy. Furthermore, the three tangential contact modes, i.e. sliding, non-sliding and loss of contacts, can be easily identified through the inequality constraints in Eq. (3.3). Note that these inequality constraints have an angular dependence through $\mathbf{n}$, such that the contact mode will vary around the particle according to the direction of contact. Therefore, the integration over all contacts in (2.1) and (2.2) can be separated into a sum of integrals, one for each contact mode. That is, Eqs. (2.1) and (2.2) may be written as

$$\sigma_{\alpha\beta} = \frac{1}{\pi R(1+\nu)}\sum_{i=1}^{T}\left[\underbrace{\int_{a_i}^{c_i} f_\alpha^{\mathrm{slid}} n_\beta \Phi\,\mathrm{d}\theta}_{\text{sliding contacts}} + \underbrace{\int_{c_i}^{d_i} f_\alpha^{\text{no slid}} n_\beta \Phi\,\mathrm{d}\theta}_{\text{non-sliding contacts}}\right], \tag{3.17}$$

$$\mu_\alpha = \frac{1}{\pi R(1+\nu)} \sum_{i=1}^{T} \left[\begin{array}{l} \displaystyle\int_{a_i}^{c_i} [M^{\text{slid}} n_\alpha + \text{Re}_{\beta\phi 3} f_\beta^{\text{slid}} n_\alpha n_\phi] \Phi \, \mathrm{d}\theta \\ \text{sliding contacts} \\ \displaystyle + \int_{c_i}^{d_i} [M^{\text{no slid}} n_\alpha + \text{Re}_{\beta\phi 3} f_\beta^{\text{no slid}} n_\alpha n_\phi] \Phi \, \mathrm{d}\theta \\ \text{non-sliding contacts} \end{array} \right]. \tag{3.18}$$

The integrals corresponding to regions of no contact are not shown, as regions of no contact do not contribute (directly) to the stress or couple stress. The summation in front of each integral is a concise representation of the multiple integrals (multiple regions of a particular contact mode) that can be encountered as $\Omega = 0 \to 2\pi$. The integration limits and the upper limit of the summation index, T, obey the following relationships:

$$\sum_{i=1}^{T} [(c_i - a_i) + (d_i - c_i) + (e_i - d_i)] = 2\pi, \quad \text{and} \quad a_1 = 0;\ a_{i+1} = e_i;\ e_T = 2\pi. \tag{3.19}$$

Eq. (3.19) is a condition that ensures that all possible contact directions ($0 \to 2\pi$) have been assigned a contact mode. In (3.19), the quantity $(e_i - d_i)$ corresponds to the range of angles for which there are no contacts. The sliding contact regions $(c_i - a_i)$ are further separated into two regions, $(b_i - a_i)$ and $(c_i - b_i)$, which are related to $\text{sign}(\Delta u^{\text{t}})$ in (3.3) being positive or negative, respectively. These integration limits are determined from the inequality constraints in (3.1) and (3.3). For example, with increasing angle a sliding contact region $(c_3 - b_3)$ is immediately followed by a region of no contact $(e_3 - d_3)$, the non-sliding contact integration limits are set to have the property $d_3 = c_3$. Due to the form of the constraints in (3.5) and (3.7), involving absolute values of cosine squared functions, there exists an upper bound on the value that the summation index T may take.

Substitution of the various contact laws presented here into (3.17) and (3.18), followed by integration, results in the following micromechanical micropolar constitutive equations:

$$\sigma_{\alpha\beta} = \frac{2Ra(\nu)}{\pi} \sum_{i=1}^{T} \left[\begin{array}{l} \dfrac{f^{\text{initial}}}{2\pi R} \left[\begin{array}{l} w_1(a_i,d_i) W_{\alpha\beta 1} + w_2(a_i,d_i) W_{\alpha\beta 2} + w_3(a_i,d_i) W_{\alpha\beta 3} \\ + \mu e_{s\alpha 3} \left[\begin{array}{l} (w_1(b_i,c_i) - w_1(a_i,b_i)) W_{s\beta 1} + (w_2(b_i,c_i) - w_2(a_i,b_i)) W_{s\beta 2} \\ + (w_3(b_i,c_i) - w_3(a_i,b_i)) W_{s\beta 3} \end{array} \right] \end{array} \right] \\ + \varepsilon_{mn} k^{\text{n}} \left[\begin{array}{l} w_4(a_i,d_i) W_{\alpha\beta 1} W_{mn1} + w_5(a_i,d_i)(W_{\alpha\beta 1} W_{mn2} + W_{\alpha\beta 2} W_{mn1}) \\ + w_6(a_i,d_i)(W_{\alpha\beta 1} W_{mn3} + W_{\alpha\beta 2} W_{mn2} + W_{\alpha\beta 3} W_{mn1}) \\ + w_7(a_i,d_i)(W_{\alpha\beta 2} W_{mn3} + W_{\alpha\beta 3} W_{mn2}) + w_8(a_i,d_i) W_{\alpha\beta 3} W_{mn3} \\ + \mu e_{s\alpha 3} \left[\begin{array}{l} (w_4(b_i,c_i) - w_4(a_i,b_i)) W_{s\beta 1} W_{mn1} \\ + (w_5(b_i,c_i) - w_5(a_i,b_i))(W_{s\beta 1} W_{mn2} + W_{s\beta 2} W_{mn1}) \\ + (w_6(b_i,c_i) - w_6(a_i,b_i))(W_{s\beta 1} W_{mn3} + W_{s\beta 2} W_{mn2} + W_{s\beta 3} W_{mn1}) \\ + (w_7(b_i,c_i) - w_7(a_i,b_i))(W_{s\beta 2} W_{mn3} + W_{s\beta 3} W_{mn2}) \\ + (w_8(b_i,c_i) - w_8(a_i,b_i)) W_{s\beta 3} W_{mn3} \end{array} \right] \end{array} \right] \\ + \varepsilon_{\alpha j} k^{\text{t}} \left[w_1(c_i,d_i) W_{j\beta 1} + w_2(c_i,d_i) W_{j\beta 2} + w_3(c_i,d_i) W_{j\beta 3} \right] \\ - \varepsilon_{sj} k^{\text{t}} \left[\begin{array}{l} w_4(c_i,d_i) W_{\alpha\beta 1} W_{sj1} + w_5(c_i,d_i) \left(\begin{array}{l} e_{h\alpha 3} W_{h\beta 1} W_{sj1} + e_{hs3} W_{\alpha\beta 1} W_{hj1} \\ + e_{h\beta 3} W_{\alpha h1} W_{sj1} + e_{hj3} W_{\alpha\beta 1} W_{sh1} \end{array} \right) \\ + w_6(c_i,d_i) \left(\begin{array}{l} W_{j\beta 1} \delta_{s\alpha} + W_{js1} \delta_{\beta\alpha} + W_{s\beta 1} \delta_{j\alpha} + W_{\alpha\beta 1} \delta_{js} \\ + W_{\alpha j1} \delta_{\beta s} + W_{\alpha s1} \delta_{\beta j} - 6 W_{\alpha\beta 1} W_{sj1} \end{array} \right) \\ + w_7(c_i,d_i) \left(\begin{array}{l} e_{h\beta 3} W_{j_{h1}} W_{s_{\alpha 3}} + e_{hj3} W_{h_{\beta 1}} W_{s_{\alpha 3}} \\ + e_{h\alpha 3} W_{sh1} W_{j_{\beta 3}} + e_{hs3} W_{h\alpha 1} W_{j_{\beta 3}} \end{array} \right) \\ + w_8(c_i,d_i)(W_{\alpha\beta 1} W_{sj1} + \delta_{j_\beta} \delta_{s_\alpha} - W_{j\beta 1} \delta_{s_\alpha} - \delta_{j_\beta} W_{\alpha s1}) \end{array} \right] \end{array} \right] \tag{3.20}$$

$$\mu_\alpha = \frac{2Ra(v)\kappa_\psi}{\pi}\sum_{i=1}^{T}\left[\begin{array}{l} k^{\text{slid}}[w_1(a_i,c_i)W_{\alpha\psi 1} + w_2(a_i,c_i)W_{\alpha\psi 2} + w_3(a_i,c_i)W_{\alpha\psi 3}] \\ +(k^{\text{no slid}} + R^2k^{\text{t}})[w_1(c_i,d_i)W_{\alpha\psi 1} + w_2(c_i,d_i)W_{\alpha\psi 2} + w_3(c_i,d_i)W_{\alpha\psi 3}] \end{array}\right], \tag{3.21}$$

where

$$\delta_{\alpha\beta} = \begin{cases} 1 & \text{if } \alpha = \beta \\ 0 & \text{if } \alpha \neq \beta \end{cases}$$

$$W_{\alpha\beta 1} = m_\alpha m_\beta$$

$$W_{\alpha\beta 2} = [e_{\phi\beta 3}W_{\alpha\phi 1} + e_{\phi\alpha 3}W_{\phi\beta 1}]$$

$$W_{\alpha\beta 3} = [\delta_{\alpha\beta} - W_{\alpha\beta 1}]$$

$$\begin{aligned} w_1(x,y) &= \frac{1}{4}(2(y-x) + (\sin 2y - \sin 2x)) \\ w_2(x,y) &= \frac{1}{4}(\cos 2x - \cos 2y) \\ w_3(x,y) &= \frac{1}{4}[2(y-x) - (\sin 2y - \sin 2x)] \\ w_4(x,y) &= \frac{1}{32}(12(y-x) + 8(\sin 2y - \sin 2x) + (\sin 4y - \sin 4x)) \\ w_5(x,y) &= \frac{1}{32}(4(\cos 2x - \cos 2y) + (\cos 4x - \cos 4y)) \\ w_6(x,y) &= \frac{1}{32}(4(y-x) - (\sin 4y - \sin 4x)) \\ w_7(x,y) &= \frac{1}{32}(-4(\cos 2y - \cos 2x) + (\cos 4y - \cos 4x)) \\ w_8(x,y) &= \frac{1}{32}(12(y-x) - 8(\sin 2y - \sin 2x) + (\sin 4y - \sin 4x)). \end{aligned} \tag{3.22}$$

Note, m_α and m_β are the α and β-components of the arbitrary unit vector $\mathbf{m}$ used as reference direction corresponding to $\theta = 0$ in the integration of (3.17) and (3.18). Furthermore, the number of contacts has been related to the local void ratio using the following expression provided by Hinrichsen et al. (1990):

$$N = \frac{1}{6-\pi\sqrt{3}}\left[36 - 4\pi\sqrt{3} - \pi^2(1+v)\right], \tag{3.23}$$

for $0 \leqslant N \leqslant 6$. Through (3.23), $a(v)$ is defined as

$$a(v) = \frac{1}{2\pi R(1+v)}\left[\frac{36 - 4\pi\sqrt{3} - \pi^2(1+v)}{6-\pi\sqrt{3}}\right]. \tag{3.24}$$

The porosity may also be related to the strain through the concepts of mass conservation by

$$v - v_0 \approx (1+v_0)[\varepsilon_{11} + \varepsilon_{22}], \tag{3.25}$$

where v_0 is the initial void ratio.

As a final note on the contact laws and the constitutive model presented in this section, it is expected that at large strains the contact laws, and therefore the constitutive model, may cease to be valid. With large strains, Δu^{n}, Δu^{t} and $\Delta\omega$ may not adequately represent the deformation occurring at a contact. Initially, contacting particles will generally move apart and form new contacts, such that the measures Δu^{n}, Δu^{t} and

$\Delta\omega$ are no longer relevant. However, the formulation provided by Tordesillas and Walsh (2002) introduces another level of subtlety. In transferring information from the discrete to the continuous, the motion of individual particles is never tracked. Instead, Tordesillas and Walsh make use of the *expectation* of finding a contact in a given direction and the behaviour of those contacts. One interpretation of this is that the contact laws should reflect the net effect of the expected contacts, just as experimental results of contact orientations reflect the average contact distribution from a large sample volume. An alternative interpretation is that the expectations are an average over all possible states that a particle can experience. Clearly, interpreting this approach in the limit of large strains is an area in need of further study. For this reason, results presented in Section 4 are arbitrarily limited to small shear strains of less than 0.4.

4. Shear band analysis and results

As mentioned earlier, one of the aims of the current paper is to demonstrate that the various evolving contact anisotropies can be predicted by the micromechanically-based constitutive model presented in Section 3. Towards this end, the one-dimensional shear band analysis first provided by Mühlhaus and Vardoulakis (1987), and later extended by Bardet and Proubet (1992) and Tordesillas et al. (in press), for a micropolar continuum subject to the bi-axial test, will be used to explore the capabilities of the micromechanically-based constitutive model in predicting shear band formation and microstructural evolution.

In the past this method for shear band analysis has been applied to micropolar constitutive models from the deformation theory of plasticity for frictional materials with internal constraint (Mühlhaus and Vardoulakis, 1987; Bardet and Proubet, 1992; Vardoulakis and Sulem, 1995). Although these constitutive models have been successful in predicting the onset and thickness of shear bands, they require a number of poorly understood fitting parameters. These fitting parameters, and therefore the constitutive models, contain no information about the particle microstructure, hence they are unable to predict microstructural evolution. In contrast to these models, the micromechanically-based constitutive model presented in Section 3 contains a direct link to the physical and measurable properties of particles (e.g. particle–particle friction coefficient, particle stiffness coefficients) and so contains no fitting parameters. All results obtained with the current model should be viewed in this light.

The shear band analysis proposed by Mühlhaus and Vardoulakis (1987) involves solving the rate form of the stress equilibrium equations for a micropolar material, and then identifying deformation solutions that may exist within a narrow region (shear band). The rate form of the stress equilibrium equations for a micropolar material is:

$$\begin{aligned}
&\left\langle \frac{\mathrm{d}\sigma_{11,1}}{\mathrm{d}t} \right\rangle + \left\langle \frac{\mathrm{d}\sigma_{12,2}}{\mathrm{d}t} \right\rangle + \sigma\left(\frac{\mathrm{d}\Gamma_{,2}}{\mathrm{d}t} \right) = 0 \\
&\left\langle \frac{\mathrm{d}\sigma_{21,1}}{\mathrm{d}t} \right\rangle + \left\langle \frac{\mathrm{d}\sigma_{22,2}}{\mathrm{d}t} \right\rangle + \sigma\left(\frac{\mathrm{d}\Gamma_{,1}}{\mathrm{d}t} \right) = 0 \\
&\left\langle \frac{\mathrm{d}\mu_{1,1}}{\mathrm{d}t} \right\rangle + \left\langle \frac{\mathrm{d}\mu_{2,2}}{\mathrm{d}t} \right\rangle + \left\langle \frac{\mathrm{d}\sigma_{21}}{\mathrm{d}t} \right\rangle - \left\langle \frac{\mathrm{d}\sigma_{12}}{\mathrm{d}t} \right\rangle = 0
\end{aligned} \tag{4.1}$$

where $\sigma = \sigma_{11} - \sigma_{22}$ and Γ represents the rigid body rotation. The angular brackets $\langle\ \rangle$ represent the Jaumann derivative of the quantity contained within. Note also that $\mathrm{d}/\mathrm{d}t$ indicates a material derivative. As depicted in Fig. 1, the proposed shear band analysis assumes that prior to shear band formation the deformation is homogeneous with no rotations. At a certain strain, a second inhomogeneous deformation with finite rotations can exist within a narrow region, called the shear band. The one-dimensional analysis assumes that all gradients are zero along the shear band. The shear band inclination angle is defined as the angle that the shear band makes with the minor principal strain axis.

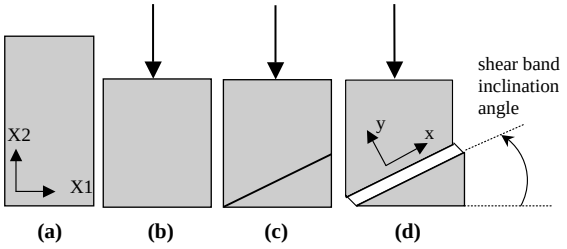

Fig. 1. Stages in shear band formation within a bi-axial test: (a) initial specimen, (b) homogeneous deformation prior to shear band formation, (c) the onset of shear banding, and (d) shear band formation. The applied compression is in the X_2 direction at a constant rate. The vertical boundaries are allowed to deform such that σ_{11} is constant at these boundaries. For the homogeneous deformation prior to shear band formation it is assumed that $\varepsilon_{12} = \varepsilon_{21} = \kappa_1 = \kappa_2 = 0$.

Inhomogeneous solutions are sought to (4.1) which satisfy the boundary conditions used by Bardet and Proubet (1992), which are consistent with the experimental observations and DEM simulations of Iwashita and Oda (2000) and Oda and Kazama (1998). These boundary conditions are as follows:

(i) Across a shear band (i.e. $-d_b \leqslant y \leqslant d_b$ where $2d_b$ is the shear band thickness), the displacement rate and the rotation rate are symmetrical in y.
(ii) $V_1 = \frac{V_1^*}{2}$ and $V_2 = \frac{V_2^*}{2}$ at $y = d_b$ and $V_1 = -\frac{V_1^*}{2}$ and $V_2 = -\frac{V_2^*}{2}$ at $y = -d_b$. Since it is assumed that regions outside the shear band act rigidly after the bifurcation strain is reached, and that the bi-axial test is strain controlled, the rate of vertical displacement of the rigid outer regions of the specimen V_2^* is prescribed. The horizontal rate of displacement V_1^*, on the other hand, needs to be determined from the strain within the shear band.
(iii) $\frac{d\omega}{dt} = 0$ at $y = d_b$ and at $y = -d_b$ and a maximum at $y = 0$.
(iv) Continuity of traction at the shear band boundary.

Once the displacement and rotation rates are determined from solving (4.1) subject to the boundary conditions, an incremental procedure is adopted to determine the strain and rotation within a shear band, and therefore the evolution of the shear band. For a complete and more detailed discussion of the shear banding problem and the method outlined here, including the incremental procedure, we refer the reader to Tordesillas et al. (in press).

One the of the main advantages of the current proposed constitutive equations is that the evolution of the contact force anisotropy and the contact anisotropy are naturally incorporated via Eqs. (3.1) and (3.3) and the contact mode transition angles a_i, b_i, c_i and d_i. In the current analysis, from the onset of deformation, the transition angles a_i, b_i, c_i and d_i are updated after each small increment of strain using the inequality constraints in (3.1) and (3.3). Hence, the characteristics of the material are updated in a stepwise manner. This enables a larger range of shear strains to be explored than an otherwise small strain analysis would allow.

Fig. 2 displays four bifurcation curves, showing the minimum shear strain ε_{11}–ε_{22} at which a shear band could potentially form at various shear band inclinations. Each curve corresponds to an initial void ratio. There are two important features to note. First, unlike our earlier model (Tordesillas et al., in press), the current constitutive equation predicts a minimum strain within each bifurcation curve. Furthermore, this minimum strain corresponds to a shear band inclination angle that is within the expected or observed shear band inclinations of 50–70°. Secondly, the void ratio is predicted to affect both the onset and inclination angle of the shear band, with denser granular materials having a delayed onset and a slightly larger inclination angle. Unfortunately, we are unaware of the existence of any experimental or simulation data that could verify this last prediction.

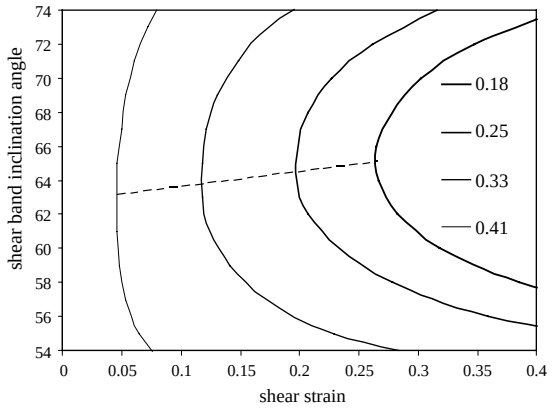

Fig. 2. Bifurcation curves for four initial void ratios: 0.18, 0.25, 0.33, 0.41. Each curve represents the minimum shear strain at which a shear band, of a particular inclination, can form. Included in this figure is a line connecting the minimum strain for each bifurcation curve. In this and, unless stated otherwise, all following figures, model parameters are $v_0 = 0.25$; $\eta = 0.05$; $k^{n} = k^{t} = 4 \times 10^{7}$ N/m; $k^{slid} = k^{no\,slid} = 7 \times 10^{2}$ N m/rad, $R = 0.005$ m. These parameters will be chosen for consistency with the parameters used in the DEM simulations of Iwashita and Oda (2000). These parameters reflect a moderate particle packing, with an initially isotropic contact and contact force distribution.

In Fig. 3, bifurcation curves are shown for three initial confinement pressures (actually $f^{initial}$). It can be seen that the average normal contact force applied to each particle prior to deformation substantially affects both the strain at the onset of shear banding and the inclination of a shear band. Specifically, the higher initial normal force delays the onset of shear banding and decreases the minimum-strain shear band inclination angle. The onset and inclination angle are also predicted to be independent of particle size.

Fig. 4 gives the prediction of how the shear band thickness evolves with shear strain. As in Fig. 2, each curve represents an initial void ratio. All but one of the curves show the shear band thickness decreasing to a steady value of approximately three particle diameters. A persistent (steady) shear band thickness is critical for consistency with the stable shear bands generally observed in experiments. The exception to the persistent shear band width is the case of an initial void ratio of 0.41, which corresponds to quite a loose

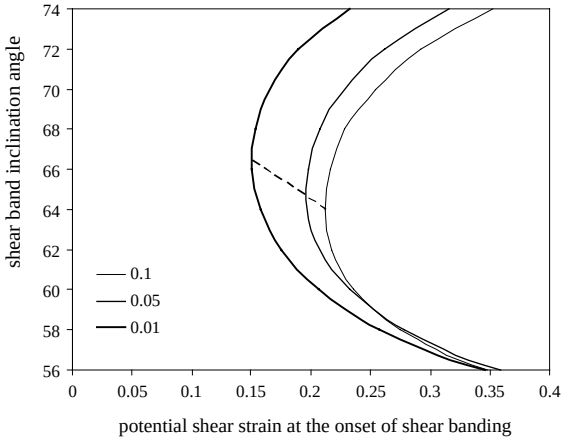

Fig. 3. Bifurcation curves for three initial normal contact forces. That is $\eta = 0.01$, 0.05 and 0.1. Included in this figure is a line connecting the minimum strain for each bifurcation curve.

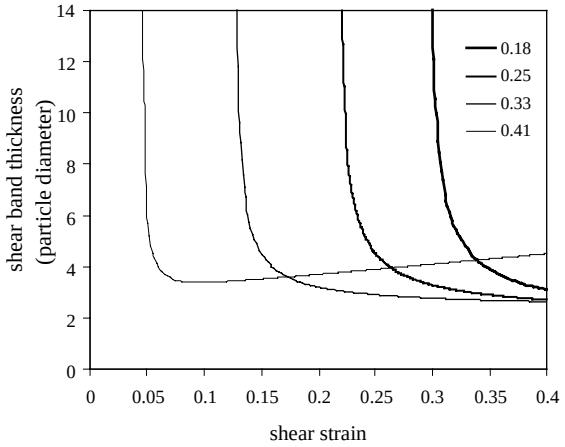

Fig. 4. Evolution of the shear band thickness with shear strain for four initial void ratios: 0.18, 0.25, 0.33, 0.41 used in Fig. 2.

sand. Note that it has been reported that shear bands in loose sands can change slightly in position, orientation and width during their evolution (see Chapter 4 of Oda and Iwashita, 1999). Perhaps the loose sand prediction seen in Fig. 4 reflects this experimental finding.

Although scaled by the particle diameter, the shear band thickness curves (in Fig. 4) are still dependent on the particle size. Fig. 5 shows the particle size dependency for the void ratio 0.25, which was one of the curves from Fig. 4. It can be seen that the constitutive model predicts the scaled shear band widths to increase with decreasing particle size, with a shear band thickness of approximately 10 particle diameters for a particle size of 1 mm. In the current model this particle size dependency originates from the contact moments i.e. terms involving $k^{\text{no slid}} + R^2 k^{\text{t}}$. Therefore, a zero rolling resistance $k^{\text{no slid}} = 0$ is the limiting case of an increasing particle size. Rolling resistance has been used in DEM simulations as a simple way of including the effects of non-circular particle shapes. It is interesting to note that the shear band thicknesses reported in real sands (7–20 particle diameters (Mühlhaus and Vardoulakis, 1987; Harris et al., 1995;

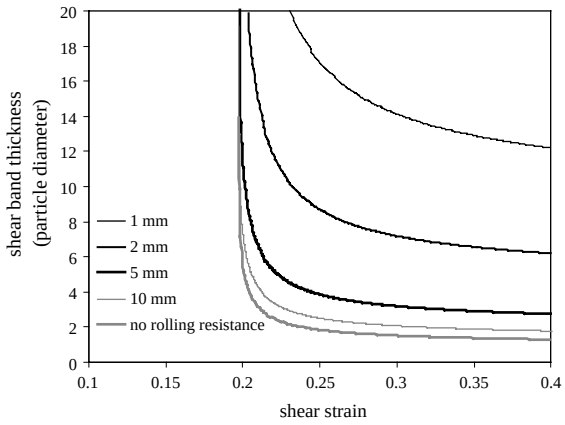

Fig. 5. Evolution of the shear band thickness with shear strain for various particle sizes. Also shown is the shear band thickness evolution for the case in which $k^{\text{slid}} = k^{\text{no slid}} = 0$. All other parameters are the same as used in Fig. 2, except the initial void ratios is 0.25.

Oda and Kazama, 1998), consisting of small non-spherical particles, are often much larger than those observed in idealised two-dimensional Schneebeli systems (1–4 particle diameters (Calvetti et al., 1997)), which consist of circular rods. This width difference may be purely due to the transition between a two-dimensional and a three-dimensional experiment, however, it would seem reasonable that the angular sand particles contribute to the thicker shear bands observed in sands. It is well known that large voids form within an evolving shear band, with a concomitant reduction in the number of contacts per particle. Force is then transmitted across a shear band through an unstable particle network. A column of particles is particularly prone to buckling via particle rotations. Therefore, for a shear band to be multiple particles wide, a rolling resistance must be present to inhibit particle rotations. That is, if rolling resistance were not present between contacting particles, long particle chains would not be present within shear bands. Unfortunately, this explanation only describes what is needed to have wide shear bands, not why shear bands are wide. In any case, the thickness predictions presented in Fig. 5 are certainly consistent with the findings reported in the literature. Note that the thickness predicted by the current model is also consistent with the shear band analysis based on the deformation theory of plasticity (Mühlhaus and Vardoulakis, 1987; Bardet and Proubet, 1992).

In Fig. 6 the change in void ratio prior to shear banding and within a shear band can be seen for the four initial void ratios examined in Figs. 2 and 3. As expected, prior to shear band formation there is compression and then within the shear band there is dilation, as revealed by the appearance of large voids within the shear band in sands (e.g. see Chapter 4 of Oda and Iwashita, 1999) and Schneebeli systems (Calvetti et al., 1997). In Fig. 6 there is also some indication of a final critical, or steady state, void ratio (Chapter 4 of Oda and Iwashita, 1999; Huang et al., 2002; Rothenburg and Kruyt, 2003), unfortunately the small strain analysis used here does not permit this to be investigated.

The results shown in Figs. 2–6 have all dealt with the continuum properties of shear bands. However, the micromechanics incorporated into Eqs. (3.20) and (3.21) provide a link to the evolution of the discrete particle microstructure and its evolution. The results presented in the remainder of this section will concentrate on the evolution of the particle fabric and the contact forces acting on particles, as predicted by the continuum constitutive model.

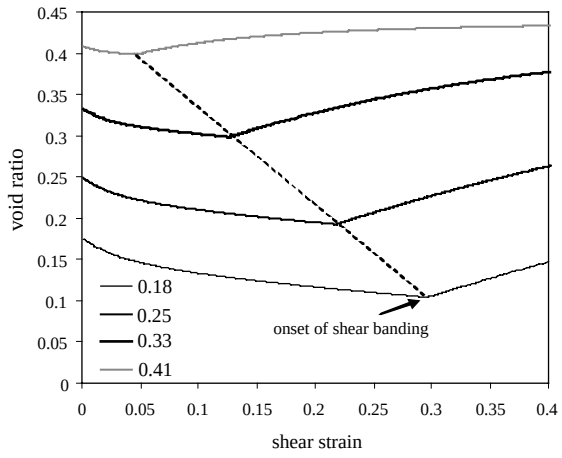

Fig. 6. Evolution of the void ratio with shear strain for four initial void ratios: 0.18, 0.25, 0.33, 0.41 used in Fig. 2. Prior to the onset of shear banding, the void ratio corresponds to the *global* void ratio. After the onset of shear banding the void ratio shown is only within the shear band or a *local* void ratio. Outside the shear band, the void ratio remains at the bifurcation level due to the rigid assumption used for these outer regions.

Still one of the clearest experimental examples of microstructural development in a bi-axial test displaying shear banding was provided by Oda et al. (1982). Using photoelastic Schneebeli rods with oval cross-sections, Oda and his co-workers observed that particles tended to align themselves in column-like structures prior to shear band formation, with both the contact directions and the normal contact forces aligned with the direction of the applied compression. That is, there is a tendency for a loss of contacts in a direction perpendicular to the applied compression, with the normal contact force being a maximum in the direction of the applied compression. This result has been reproduced many times in other experiments and DEM simulations (e.g. Bardet and Proubet, 1991; Iwashita and Oda, 2000; Rothenburg and Bathurst, 1993; Sidoroff et al., 1993; Kruyt and Rothenburg, 2003). Typically, the contact distribution is found to be of the bipolar form given by Eq. (2.4). Furthermore, the normal contact force is also found to have this bipolar form. In the bi-axial DEM simulations of Rothenburg and Bathurst (1993); Sidoroff et al., 1993); Kruyt and Rothenburg (2003), the tangential contact force is seen to contain four lobes with a minimum tangential contact force in directions both parallel and perpendicular to the applied normal compression.

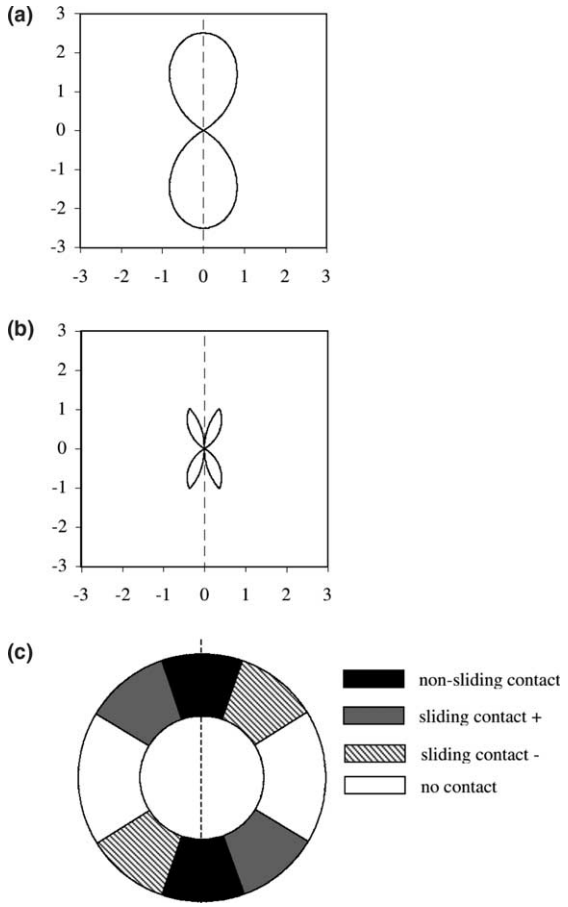

Fig. 7. Contact forces and contact modes at the onset of shear banding for the shear band evolution presented in Fig. 4 with a void ratio of 0.25. (a) is a polar plot showing the normal contact force and is normalised by the current average normal contact force. (b) is a polar plot showing the tangential contact force and is also normalised by the current average *normal* contact force. (c) shows the variation in the contact modes around a particle. The vertical dashed line indicates the direction of the applied compression. The sliding contacts have been separated into two regions depending on $\text{sign}(\Delta u^{\text{t}})$.

For both the normal and tangential contact forces these studies observed that after an initial increase in anisotropy, the degree of anisotropy then decreases.

Fig. 7 shows the normal contact force, the tangential contact force and the contact modes at the onset of shear banding. The contact force graphs have been scaled by the current average normal contact force. The first thing of note is that the constitutive model is able to predict both a contact and a contact force anisotropy arising from an initially isotropic contact distribution. Furthermore, the degree, shape and alignment of contacts and the contact force anisotropy are generally consistent with those seen in experiments and simulations of bi-axial compression discussed previously. However, there are some differences between the predicted distributions and those seen in experiments and simulations. Firstly, the degree of the predicted contact force anisotropies does not decrease after initially increasing. This highlights a limitation of the model at larger strains, associated with its current inability to incorporate the formation of new contacts. Secondly, the predicted contact distributions have no contacts in the direction perpendicular to the applied compression, whereas experiments and DEM simulations always find contacts in these directions. It is thought that this difference is due to the one-dimensional nature of the shear band analysis used. If the one-dimensional analysis was relaxed, such that a variation in void ratio and strain could occur both

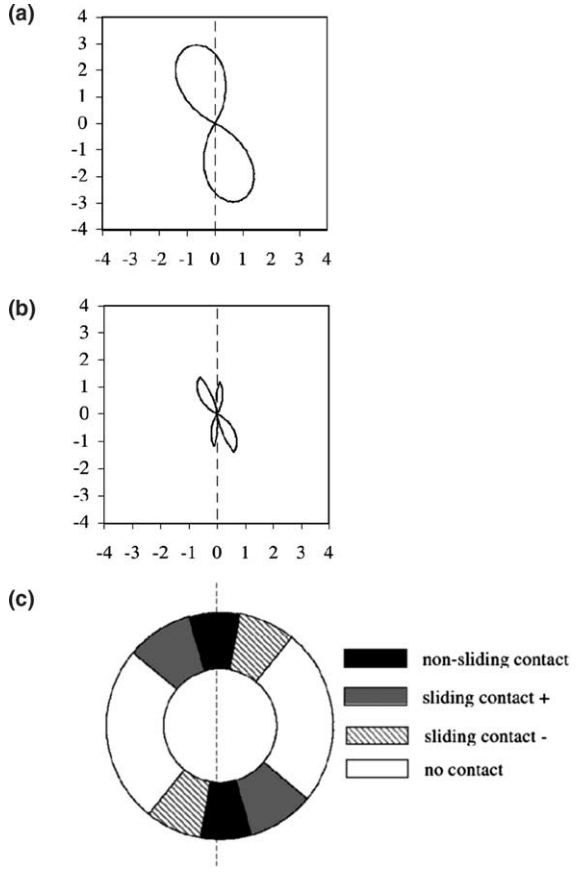

Fig. 8. Contact forces and contact modes at a shear strain of 0.4 for the bi-axial test and shear band presented in Fig. 7. (a) is a polar plot showing the normal contact force and is normalised by the current average normal contact force. (b) is a polar plot showing the tangential contact force and is also normalised by the current average *normal* contact force. (c) shows the variation in the contact modes about a particle. The vertical dashed line indicates the direction of the applied compression.

across the shear band and along the shear band, the average contact orientations from the whole specimen would likely result in finite contacts perpendicular to the applied compression. It is the goal of future work to test the current constitutive model in a 2D micropolar finite element analysis.

Based on his earlier experiments (Oda et al., 1982), Oda and Kazama (1998) proposed that the formation of shear bands coincides with the buckling of the particle columns, through particle rotation rather than sliding, with particles predominately rotating in the same direction. It may also be concluded, from viewing the images from the 1982 experiments and Iwashita and Oda's (2000) DEM simulations, that the direction of the contacts and maximum normal contact force rotates away from the direction of the applied compression, such that contacts are maintained across the shear band and generally lost along the shear band. The contact evolution within the shear band is shown in Fig. 8. Consistent with the previously discussed experiments and simulations, within the shear band, it can be seen that the contact orientations and the normal contact force are predicted to rotate away from the direction of the applied vertical deformation, with even more contacts lost in a direction along the shear band. Furthermore, in keeping with Oda and Kazama's (1998) buckling mechanism for shear band formation, which highlighted the importance of rolling (not sliding), non-sliding contact regions are predicted to be present, in conjunction with unidirectional rotations (see Fig. 9).

Although not clear in Figs. 7 and 8, the magnitude of the maximum normal contact force continues to increase beyond shear band formation, despite the fact that shear bands are a softening mechanism. Indeed softening does occur after the onset of shear banding in the current analysis. It is important to realise that the stress in the region of a particle is not necessarily related to the maximum contact force on the particle. For example, inside a shear band the void ratio increases and the number of contacts decrease, hence fewer particle contacts are available to transmit force and the average force on each contact within a shear band can increase. This is supported by the higher fringe intensity of photoelastic discs observed inside the shear bands in Oda et al. (1982) experiments, in comparison to discs outside the shear band. Of course, as mentioned at the end of Section 2, there is always room to question the viability of the simple contact laws at larger strain.

The total rotation in the region of the shear band, as shown in Fig. 9, refers to the net accumulation of rotation ω since the onset of shear banding. The total rotation is determined from accumulating (adding) the rotation from all previous strains up until the final strain, which is 40% in this figure. This accumulated

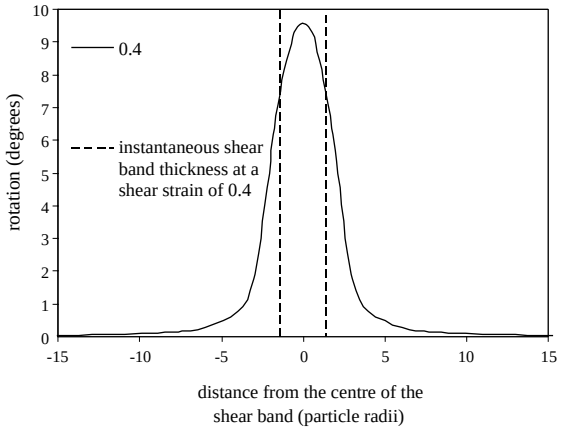

Fig. 9. Total (accumulated) rotation in the region of the shear band after a shear strain of 0.4, for the bi-axial test and shear band presented in Figs. 7 and 8. Also shown using vertical lines is the thickness of a shear band at a shear strain of 0.4, as would be given by Fig. 4 for example.

rotation is equivalent to the disturbance, or particle rotations, recorded in experiments. Note that if one were to measure the thickness of a shear band based on strain gradients, or instantaneous deformation, as done in Figs. 4 and 5, the recorded thickness would be less than the thickness measured by taking the overall disturbance to the material. For example, although the shear band thickness at a shear strain of 0.4 is only 2–3 particle diameters (Fig. 4), the microstructure beyond three particle diameters has been disturbed (finite rotations) due to prior shear strains for which the shear band thickness was greater than three particle diameters. The shear band thickness shown in Fig. 4 should then be considered an instantaneous thickness, whereas a shear band thickness implied by rotations would better represent those recorded in experiments.

The first thing to note in Fig. 9 is that the rotations are predicted to be unidirectional, consistent with the DEM simulations of Iwashita and Oda (2000). Furthermore, the maximum rotations are of the same order as those observed in experiments (the actual value is a function of the degree of deformation). In our previous constitutive model (Tordesillas et al., in press), the shear bands were generally short lived and, consequently, the accumulated rotations were much smaller than expected. The shear band thickness determined from the accumulated rotations is approximately twice the width, or 4–6 particle diameters, as those determined from the instantaneous shear band thickness shown in Fig. 4.

As a final remark, on some scale, it is inevitable that the inhomogeneous nature of the assembly is lost as a result of a continuum model formulation. Variations from the mean-field estimations can have a significant effect on the behaviour of an assembly. However, the large scatter or fluctuations in particle rotations and displacement about their mean value can be addressed using the principles of thermomechanics or "internal variable theory". By building on the earlier work of Valanis (1996), Walsh and Tordesillas (2004) showed how these fluctuations could be incorporated into the micromechanical model in a way that is consistent with the laws of thermodynamics.

5. Conclusions

Many of the observed features of shear band formation and evolution have been predicted here using a micromechanically-based, micropolar constitutive model within a simple (one-dimensional) shear band analysis, including microstructural evolution such as contact and contact force anisotropy evolution. It is important to emphasize that these results were obtained without resorting to any poorly understood fitting parameters, as would be found in a more phenomenological model. It is this last point that encourages our future research and the implementation of this model within a less restrictive numerical framework.

Acknowledgements

The authors gratefully acknowledge the support of the US Army Research Office under grant number DAAD19-02-1-0216 and the Melbourne Research Development Grant Scheme. Furthermore, we wish to thank our reviewers and Dr. Katalin Bagi for their helpful comments and suggestions.

References

Bagi, K., 1996. Stress and strain in granular assemblies. Mechanics of Materials 22, 165–177.

Bardet, J.P., Proubet, J., 1991. A numerical investigation of the structure of persistent shear blends on granular media. Geotechnique 41 (4), 599–613.

Bardet, J.P., Proubet, J., 1992. Shear-band analysis in idealized granular material. Journal of Engineering mechanics 118, 397–415.

Bardet, J.P., Vardoulakis, I., 2001. The asymmetry of stress in granular media. International Journal of Solids and Structures 38, 353–367.

Calvetti, F., Combe, G., Lanier, J., 1997. Experimental micro-mechanical analysis of a 2D-granular material: relation between structure evolution and loading path. Mechanics of Cohesive-Frictional Materials 2, 121–163.

Chang, C.S., Ma, L., 1991. A micromechanically-based micropolar theory for deformation of granular solids. International Journal of Solids and Structures 21, 67–86.

Dedecker, F., Chaze, M., Dubujet, Ph., Cambou, B., 2000. Specific features of strain in granular materials. Mechanics of Cohesive-Frictional Materials 5, 173–193.

Harris, W.W., Viggiani, G., Mooney, M.A., Finno, R.J., 1995. Use of stereophotogrammetry to analyze the development of shear bands in sand. Geotechnical Testing Journal 18, 405–420.

Hinrichsen, H.J., Feder, J., Jøssang, T., 1990. Random packing of disks in two dimensions. Physical Review A 41, 4199–4209.

Huang, W., Nübel, K., Bauer, E., 2002. Polar extension of a hypoplastic model for granular materials with shear localization. Mechanics of Materials 34, 563–576.

Iwashita, K., Oda, M., 2000. Micro-deformation mechanism of shear banding process based on modified distinct element method. Powder Technology 109, 192–205.

Kruyt, N.P., Rothenburg, L., 2003. Statistics of forces and relative displacements at contacts in biaxial deformation of granular materials. In: Bagi, K. (Ed.), Proceedings of the QuaDPM'03 Workshop. Publishing company of BUTE, Budapest, pp. 141–150.

Luding, S., 2003. Micro–macro transition for anisotropic granular packing. In: Bagi, K. (Ed.), Proceedings of the QuaDPM'03 Workshop. Publishing company of BUTE, Budapest, pp. 167–178.

Mühlhaus, H.B., Vardoulakis, I., 1987. The thickness of shear bands in granular materials. Geotechnique 37, 271–283.

Nouguier-Lehon, C., Cambou, B., Vincens, E., 2003. Anisotropy induced by particle shape in granular materials. In: Bagi, K. (Ed.), Proceedings of the QuaDPM'03 Workshop. Publishing company of BUTE, Budapest, pp. 61–69.

Oda, M., Konishi, J., Nemat-Nasser, S., 1982. Experimental micromechanical evaluation of the strength of granular materials: Effects of particle rolling. Mechanics of Materials 1, 269–283.

Oda, M., Iwashita, K. (Eds.), 1999. Mechanics of Granular Materials: An Introduction. A.A. Balkema, Rotterdam.

Oda, M., Kazama, H., 1998. Microstructure of shear bands and its relation to the mechanisms of dilatency and failure of dense granular soils. Geotechnique 48, 465–481.

Rothenburg, L., Bathurst, R.J., 1993. Influence of particle eccentricity on micromechanical behavior of granular materials. Mechanics of Materials 16, 141–152.

Rothenburg, L., Bathurst, R.J., Dusseault, M.B., 1989. Micromechanical ideas in constitutive modelling of granular materials. In: Biarez, J., Gourves, R. (Eds.), Powders and Grains. Balkema, Rotterdam, pp. 355–363.

Rothenburg, L., Kruyt, N.P., 2003. Micromechanical study of critical state in granular materials. In: Bagi, K. (Ed.), Proceedings of the QuaDPM'03 Workshop. Publishing company of BUTE, Budapest, pp. 203–212.

Sidoroff, F., Cambou, B., Mahboubi, A., 1993. Contact force distribution in granular media. Mechanics of Materials 16, 83–89.

Tordesillas, A., Walsh, S.D.C., 2002. Incorporating rolling resistance and contact anisotropy in micromechanical models of granular media. Powder Technology 124, 106–111.

Tordesillas, A., Peters, J.F., Gardiner, B.S. Insights on 1D localisation theory and micromechanical constitutive laws. Geotechnique, in press.

Tordesillas, A., Peters, J.F., Gardiner, B.S., 2003. Shear band evolution and accumulated microstructural development in Cosserat Media. International Journal for Numerical and Analytical Methods in Geomechanics.

Walsh, S.D.C., Tordesillas, A., 2002. Stranger than friction—micromechanics of granular media. In: Proceedings, 14th International Conference of the ISTVS, Vicksburg.

Walsh, S.D.C., Tordesillas, A., 2004. A thermomechanical approach to the development of micropolar constitutive models of granular media. Acta Mechanica 167 (3–4), 145–169.

Vardoulakis, I., Sulem, J., 1995. Bifurcation Analysis in Geomechanics. Blackie Academic and Professional, Glasgow.

Valanis, K.C., 1996. Gradient theory of internal variables. Acta Mechanica 116, 79–93.